Statistical Rate Theory Examination of Ethanol Evaporation

ARTICLE *in* THE JOURNAL OF PHYSICAL CHEMISTRY B · MAY 2010

Impact Factor: 3.3 · DOI: 10.1021/jp100441m · Source: PubMed

2 AUTHORS:

Aaron H Persad
University of Toronto
5 PUBLICATIONS **14** CITATIONS
SEE PROFILE

Charles Albert Ward
University of Toronto
141 PUBLICATIONS **2,587** CITATIONS
SEE PROFILE

Statistical Rate Theory Examination of Ethanol Evaporation

A. H. Persad and C. A. Ward*

Thermodynamics and Kinetics Laboratory, Department of Mechanical and Industrial Engineering, University of Toronto, Toronto, Canada M5S 3G8

Received: January 16, 2010; Revised Manuscript Received: March 10, 2010

A series of low-temperature ($246 < T_I^L < 267$ K) steady-state ethanol evaporation experiments have been conducted to determine the saturation vapor pressure of metastable ethanol. The measured interfacial conditions have been used with statistical rate theory (SRT) to develop an expression for the saturation vapor pressure as a function of temperature, f_{srt}^{eth}. This expression is shown to be thermodynamically consistent because it gives predictions of both the evaporative latent heat and the liquid constant-pressure specific heat that are in agreement with independent measurements of these properties. In each experiment, the interfacial vapor temperature was measured to be greater than the interfacial liquid temperature, $\equiv \Delta T_I^{LV}$. When f_{srt}^{eth} is used in SRT to predict ΔT_I^{LV}, the results are shown to be consistent with the measurements. Other expressions for the saturation vapor pressure that are in the literature are examined and found to be thermodynamically inconsistent and do not lead to valid predictions of ΔT_I^{LV}.

I. Introduction

The saturation vapor pressure of a pure substance, $P_s(T)$, is defined as the pressure at which equilibrium would exist between the liquid and vapor phases of the substance if the phases were maintained at the same temperature, T, and pressure, P. If there is no net phase change taking place, $P_s(T)$ is an equilibrium property. However, if a phase change process is occurring, there is often a temperature discontinuity at the interface.[1−3] If local equilibrium is assumed to exist within each phase, there are then two saturation vapor pressures defined, one in each phase.

It has been demonstrated that pure water can remain liquid down to 253 K while evaporating steadily into its own vapor.[4,5] The conventional method of measuring $P_s(T)$ for water at temperatures significantly below 273 K is difficult to apply because water is metastable and has a propensity to freeze at these conditions. However, $P_s(T)$ is defined for metastable liquids and is often used as the reference condition for the chemical potentials of the liquid and vapor phases, μ^L and μ^V, respectively. The saturation vapor pressure would be the pressure for which

$$\mu^L[T, P_s(T)] = \mu^V[T, P_s(T)] \quad (1)$$

Note that $P_s(T)$ may be defined at any temperature. Also, the $P_s(T)$ expression can be used to predict the latent heat of evaporation, $h_{fg}(T)$, and a relation between the constant-pressure specific heats of the liquid and vapor phases (see below). Thus, the thermodynamic consistency of a proposed $P_s(T)$ relation may be examined experimentally.[4]

As has been illustrated for water,[4] one way in which the saturation vapor pressure of a liquid in a metastable state may be determined is from phase change experiments and the application of statistical rate theory (SRT).[6−8] For each of 50 phase change experiments conducted over a range of interfacial liquid temperatures, the value of $P_s(T)$ was determined and expressed as a function of temperature

$$P_s(T) = f_{srt}^{H_2O}(T) \quad (2)$$

and this expression for $P_s(T)$ of water was found to be thermodynamically consistent.

In the SRT approach, the evaporation flux is predicted to depend on the change in entropy that results from one molecule transferring spontaneously from the liquid to the vapor phase, Δs_{lv}. If the vapor phase is approximated as an ideal gas of nonlinear molecules that consists of n atoms, then a molecule can have $3n - 6$ internal molecular vibration frequencies (molecular phonons[9]). Fang and Ward[1,10] considered the evaporation of water, methylcyclohexane, and octane. The molecular phonons of water were known, but those for methylcyclohexane and octane were not. For these latter two substances, they approximated the vapor phase as ideal and the liquid as incompressible and neglected the molecular phonons, but nonetheless, for a series of measured evaporation fluxes, they were able to predict the vapor-phase pressures that were in agreement with those measured.

For octane, ethane, butane, and water, Kapoor and Elliott[11] calculated the vapor-phase pressure using SRT and the Peng−Robinson equation of state.[12] This equation can be used to describe both the liquid and vapor phases. Kapoor and Elliott neglected the phonons and the interfacial temperature discontinuities. When their calculated pressures were compared with those obtained from SRT with the vapor approximated as an ideal gas and the liquid phase as incompressible, Kapoor and Elliott found some differences for ethane and butane at high evaporation rates, but no differences were found for octane or water. Their sensitivity analysis indicated that for butane, an interfacial temperature discontinuity of less than 2 K made little difference in the calculated vapor-phase pressures.

During water evaporation studies in which the vapor phase was heated electrically, Badam et al.[13,14] found much larger interfacial temperature discontinuities; the interfacial vapor temperature was measured to be as much as 27.83 K greater than the interfacial liquid temperature. With the expression for $P_s(T)$ given in eq 2, SRT was used to predict the interfacial

* To whom correspondence should be addressed. E-mail: charles.ward@utoronto.ca.

10.1021/jp100441m
Published on Web 04/20/2010

temperature discontinuities of up to 15.7 K. The higher interfacial temperature discontinuities could not be predicted because a pressure transducer failed in these experiments, and knowledge of the vapor-phase pressure is essential for predicting the interfacial temperature discontinuities.[9]

These extraordinary interfacial temperature discontinuities then are consistent with SRT, provided a thermodynamically consistent expression for $P_s(T)$ is included in the calculation procedure. The question of the molecular mechanism by which such large temperature discontinuities could exist under steady-state conditions has not been established. In this study, we examine the evaporation of another fluid, ethanol. From steady-state evaporation experiments conducted in the range of $246 < T_I^L < 267$ K, we first determine a thermodynamically consistent expression for $P_s(T)$ by using SRT. Other presently available expressions for $P_s(T)$[15−17] are shown not to be thermodynamically consistent in this temperature range. We then show that the inconsistent expressions for $P_s(T)$ do not lead to valid predictions of the measured interfacial temperature discontinuities.

A. Statistical Rate Theory. On the centerline of an axisymmetric liquid phase undergoing a steady-state phase change, surface-tension-driven convection may be neglected, and if the temperature gradients in each phase are measured, the evaporation flux at this position, j_{ev}^0, may be determined from the conservation-of-energy principle[3,18]

$$j_{ev}^0 = \frac{1}{h^V(T_I^V) - h^L(T_I^L)}(-\kappa^L \nabla T^L \cdot i_r + \kappa^V \nabla T^V \cdot i_r) \tag{3}$$

where h^i is an enthalpy, κ^i is a thermal conductivity, a superscript L or V refers to a property of the liquid or vapor phase, respectively, and superscript I refers to a property of the interface in a phase.

From SRT, one finds that the evaporation flux is given by[8]

$$j_{ev} = 2K_e \sinh\left(\frac{\Delta s_{lv}}{k_b}\right) \tag{4}$$

where

$$K_e = \frac{\eta P_s(T_I^L)}{\sqrt{2\pi m k_b T_I^L}} \tag{5}$$

$$\eta = \exp\left[\frac{v_f(T_I^L)}{k_b T_I^L}(P_e^L - P_s(T_I^L))\right] \tag{6}$$

$$\frac{\Delta s_{lv}}{k_b} = \ln\left[\left(\frac{T_I^V}{T_I^L}\right)^4 \frac{P_s(T_I^L)}{P_I^V}\right] + \ln\left[\frac{q_{vib}(T_I^V)}{q_{vib}(T_I^L)}\right] + 4\left(1 - \frac{T_I^V}{T_I^L}\right) + \left(\frac{1}{T_I^V} - \frac{1}{T_I^L}\right)\sum_{l=1}^{3n-6}\left[\frac{\theta_l}{2} + \frac{\theta_l}{e^{\theta_l/T_I^V} - 1}\right] + \frac{v_f(T_I^L)}{k_b T_I^L}[P_I^V + \gamma^{LV}(T)(C_1 + C_2) - P_s(T_I^L)] \tag{7}$$

$$\theta_l = \frac{\hbar \omega_l}{k_b} \tag{8}$$

$$q_{vib}(T) = \prod_{l=1}^{3n-6} \frac{e^{-\theta_l/2T}}{1 - e^{-\theta_l/T}} \tag{9}$$

and P_e^L must satisfy

$$P_e^L - \gamma^{LV}(T)(C_1 + C_2) = \eta P_s(T_I^L) \tag{10}$$

where k_b is the Boltzmann constant, $\hbar$ is the reduced Planck constant, m is the mass of a molecule undergoing evaporation, ω_l is a molecular phonon, v_f is the specific volume of the liquid at saturation, γ^{LV} is the surface tension at the liquid−vapor interface, and P_e^L is the liquid pressure that would exist at equilibrium. If the liquid−vapor interface is spherical, then the sum of curvatures of the interface, $C_1 + C_2$, may be replaced with $2C_0$, where C_0 is the curvature of the spherical interface.

If the molecular phonons of the evaporating molecule are known, then by measuring j_{ev}^0 at a series of conditions, the values of $P_s(T_I^L)$ may be determined at each condition, and a fitting relation, f_{srt}^r, is formulated giving

$$P_s(T) = f_{srt}^r(T) \tag{11}$$

where r denotes the chemical species undergoing the phase change process.

The expression for $P_s(T)$ obtained by this procedure may be examined by using it to predict both the evaporative latent heat, $h_{fg}(T)$, and the constant-pressure specific heat of the liquid, $c_p^L(T)$[4]

$$h_{fg}(T) = T(v_g(T) - v_f(T))\frac{df_{srt}^r}{dT} \tag{12}$$

$$c_p^L(T) = c_p^V(T) - \frac{d}{dT}\left(\frac{\bar{R}T^2}{f_{srt}^r}\frac{df_{srt}^r}{dT}\right) \tag{13}$$

where $\bar{R}$ is the gas constant.

Provided that the constant-pressure specific heat of the vapor, $c_p^V(T)$, is known, the expression for $f_{srt}^r(T)$ may be used to calculate the values of both $h_{fg}(T)$ and $c_p^L(T)$ as functions of T. Thus, the consistency of the values of the properties calculated from the expression for f_{srt}^r may be evaluated by comparing the predicted values of these properties with independent measurements of $h_{fg}(T)$ and $c_p^L(T)$. Further, other proposed expressions for $P_s(T)$ may be examined by using them to predict these properties.

B. Motivation for Studying Ethanol at Low Temperatures. Many expressions for $P_s(T)$ of ethanol presently exist. Three of the ones found in the literature are from (1) the Design Institute for Physical Properties Research (DIPPR) Project 801; this compilation was obtained from several data sets that span many decades;[15] (2) Yaws' Handbook, which is also a compilation of data sets and spans a similar temperature range[16] as that of DIPPR; and (3) Dillon and Penoncello, who formulated an expression using data that is more recent but none below 273 K.[17] The two data points[15,19] presently available below 273 K are shown as black dots in Figure 1. Also shown in this figure are the available $P_s(T)$ expressions from these three sources. Note that there is no experimental data between 243 and 273 K, even though both DIPPR and Yaws claim that their $P_s(T)$ expressions are valid down to 159 K.[15,16]

As seen in Figure 1, despite the small amount of low-temperature data available in the literature, all three of the presently available $P_s(T)$ expressions appear consistent with each other, and each fits the two data points well.

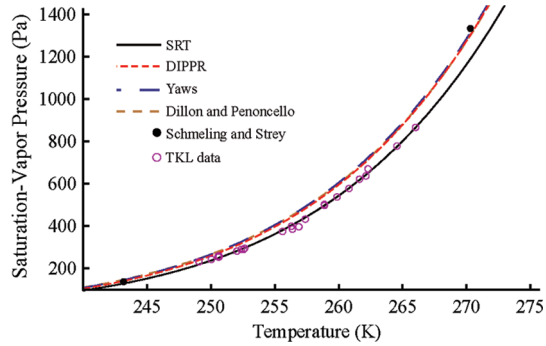

Figure 1. The measurements of the saturation vapor pressure of ethanol at low temperatures that have been reported in the literature are shown as black dots, and those obtained in this study are shown as open circles. Also shown are the values calculated from the $P_s(T)$ expressions available in the literature and the values obtained for $f_{srt}^{eth}(T)$.

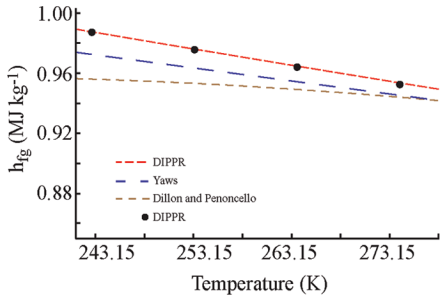

Figure 2. The measurements of the evaporative latent heat of ethanol at low temperatures that have been reported in the literature are shown. Also shown are the values calculated from the $P_s(T)$ expressions available in the literature. Note that the values of $h_{fg}(T)$ calculated from the DIPPR expression for $P_s(T)$ are consistent with the available data but that the calculations from the relations of Yaws and of Dillon and Penoncello are not.

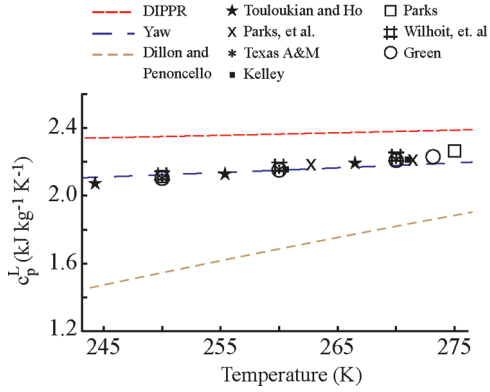

Figure 3. The measurements of $c_p^L(T)$ at low temperatures that have been reported in the literature are shown. Also shown are the values calculated from the three expressions for $P_s(T)$ that are presently available in the literature. Note that only the Yaws expression for $P_s(T)$ leads to valid predictions of $c_p^L(T)$.

However, the three presently available analytical expressions for the $P_s(T)$ of ethanol have different slopes. The calculated values of $h_{fg}(T)$ and $c_p^L(T)$ obtained from eqs 12 and 13 are shown in Figures 2 and 3, respectively. As indicated in Figure 2, of the three expressions, only the DIPPR expression leads to predictions of $h_{fg}(T)$ that are in agreement with the independent measurements. However, as seen in Figure 3, the DIPPR expression predicts $c_p^L(T)$ values that disagree with the independent measurements of this property. Thus, these results indicate that none of the presently available expressions for $P_s(T)$ lead to consistent predictions of both $h_{fg}(T)$ and $c_p^L(T)$ in the temperature range considered and therefore are viewed as thermodynamically inconsistent.

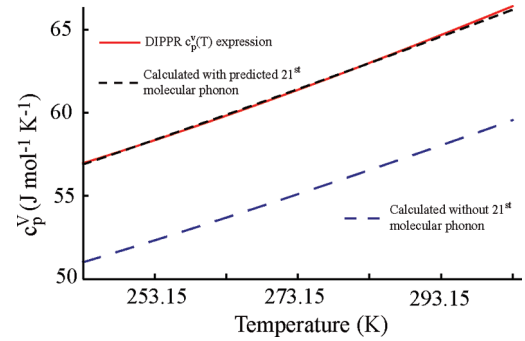

Figure 4. Comparison of the experimental values of $c_p^V(T)$[15] with the values calculated with and without the ω_{21} in eq 14. The value obtained for ω_{21} is 350 cm^{-1}.

C. Molecular Phonons of Ethanol. Ethanol (CH_3CH_2OH) is a nonlinear molecule and has 21 molecular phonons.[20,21] Two of these frequencies are due to the internal rotations of the CH_3 and OH groups and cannot be easily determined from infrared or Raman spectroscopy. The values of the remaining 19 phonons reported in the literature are somewhat scattered, which is in part due to different conformations of ethanol and the hydrogen bonding between ethanol molecules.[20−24]

In this study, the molecular phonons reported by Green[21] are used; the five CH stretching modes are each assigned at 2989 cm^{-1}, the OH stretching mode is assigned at 3689 cm^{-1}, the pair of antisymmetric CH_3 deformations and the CH_2 bending mode are approximated as 1456 cm^{-1}, the symmetric CH_3 deformation is placed at 1391 cm^{-1}, the COH deformation is at 1242 cm^{-1}, the CH_2 rocking, wagging, and twisting modes are at 801, 1320, and 1270 cm^{-1}, respectively, the CO and CC stretching frequencies are at 1067 and 877 cm^{-1}, respectively, the CCO skeletal deformation is assigned as 427 cm^{-1}, while the rocking modes of CH_3 are at 1040 and 1104 cm^{-1}. Green suggests that a value of 267 cm^{-1} can be adopted for the torsional vibration frequency of the methyl group. Thus, only the torsional vibration frequency of the hydroxyl group remains unknown.

Since the vapor-phase constant-pressure specific heat, $c_p^V(T)$, of ethanol is sensitive to the phonons of the molecule, the unknown frequency can be found using the measurements of $c_p^V(T)$ given in DIPPR[15] and eq 14[25]

$$c_p^V(T) = \bar{R} + k_b\left(3 + \sum_{l=1}^{3n-6}\left(\frac{\hbar\omega_l}{k_bT}\right)^2\frac{e^{\hbar\omega_l/k_bT}}{(e^{\hbar\omega_l/k_bT}-1)^2}\right) \quad (14)$$

When the values of the phonons reported by Green[21] are inserted into eq 14, there is only one unknown in the equation, ω_{21}. As indicated in Figure 4, the value ω_{21} may be chosen so that the value of c_p^V calculated from eq 14 agrees with the measurements[15] throughout the temperature range. The value obtained is 350 cm^{-1}, and it is within the possible range of 195−403 cm^{-1} reported for the hindered torsional vibration frequency of the hydroxyl group in ethanol.[26] Thus, all 21 molecular phonons of ethanol to be used in this study are now known.

II. Experimental Apparatus and Methods for the Kinetic Experiments

The apparatus to be used in the experiments is shown schematically in Figure 5. Once the apparatus had been prepared,

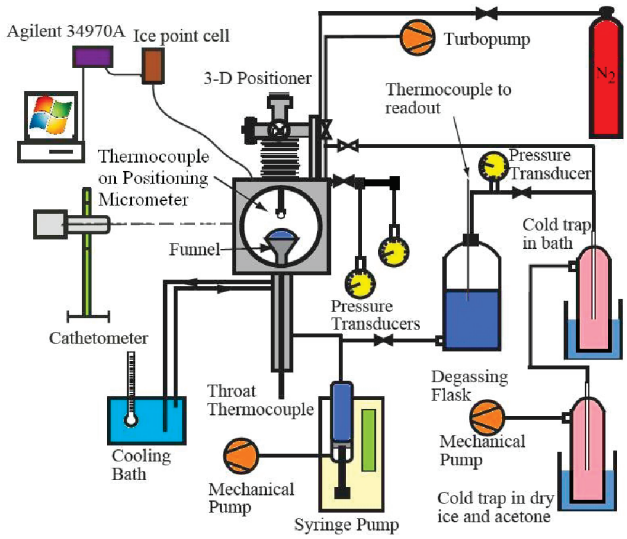

Figure 5. Schematic of the experimental apparatus used to conduct steady-state evaporation studies.

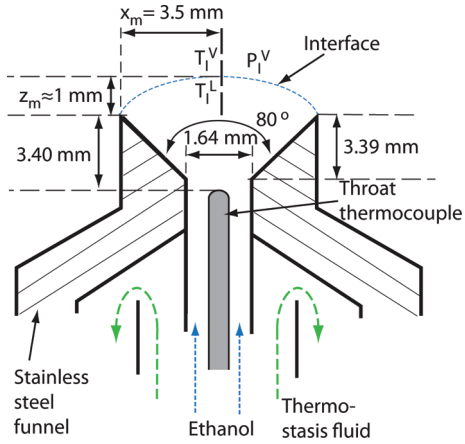

Figure 6. Schematic of the stainless-steel funnel.

the ethanol was pumped into the throat of a stainless-steel funnel and maintained at the mouth as it evaporated steadily.

A. Preparation Procedure. The pure water used for cleaning was deionized, distilled, and nanofiltered and had a resistivity of at least 18.2 MΩ·cm. All chamber components to be exposed to ethanol were first cleaned using the following procedure. The stainless steel and glass materials were soaked in acetone (VWR, 99.5%) for 24 h and thoroughly rinsed with pure water. This was followed by a bath in detergent (Alconox) for 24 h and a thorough rinse with pure water. Glass materials were additionally soaked in chromic sulfuric acid (VWR, 99.9%) for 24 h, thoroughly rinsed with pure water, and finally rinsed with pure anhydrous ethanol twice. All other materials were cleaned by soaking in detergent for 24 h, followed by a thorough rinsing with pure water.

The evaporation experiments were performed in a cubical stainless-steel-vacuum chamber (see Figure 5). A stainless-steel funnel was positioned in the center of the chamber. A diagram of the funnel is shown in Figure 6. The funnel had a mouth opening of 7 mm and a volume of 0.05 mL. The throat of the funnel was enclosed in a heat exchanger. A syringe micropump was connected to the throat of the funnel. The syringe was directly connected to a glass degassing flask. The evaporation chamber and a glass syringe were evacuated with a turbomolecular diffusion pump (Leybold, UHV1100) for at least 24 h. The chamber pressure was $\sim 10^{-5}$ Pa. The vapor phase was monitored with a quadrupole residual gas analyzer (SRS, RGA200) to test for any impurities in the chamber.

Pure anhydrous ethanol (Chemical Alcohols, 100%) was introduced into the degassing flask and degassed for at least 8 h while being stirred. The degassed ethanol was transferred directly into the syringe without exposure to air.

B. Evaporation under Steady-State Conditions. Ethanol was pumped from the syringe into the funnel throat until the height of the ethanol above the funnel mouth was ∼1 mm. At this height, the Bond number was less than unity, and the liquid−vapor interface could be approximated as spherical.[27] The interface was viewed through two glass view ports separated by 90° using a cathetometer (PTI, 2212) and a telescope. The cathetometer had a positioning accuracy of ±10 μm. Light sources were located at the other view ports. The light sources had filters to diffuse the light and reduce the amount of heat reaching the chamber.

To prevent bubble formation after introducing the ethanol into the funnel, the chamber was pressurized with N_2 to ∼140 kPa for at least 4 h. Afterward, 2.5 mL of liquid was flushed out of the funnel to remove any ethanol containing dissolved N_2. The chamber was then dried with the mechanical vacuum pump (Welch, 1402) while keeping the funnel filled with ethanol. The mechanical vacuum pump was separated from the chamber by two cold traps in series. The temperature of the cold trap closest to the chamber was ∼215 K. The purpose of this cold trap was to condense the ethanol vapor and prevent it from affecting the mechanical vacuum pump's performance. The second cold trap was submerged in a mixture of acetone and dry ice and maintained at a temperature near 195 K. This cold trap would condense any oil vapor that may have diffused from the mechanical vacuum pump, thus preventing it from entering into the evaporation chamber.

With degassed ethanol in the funnel, the pressure in the chamber was slowly reduced with a leak valve and mechanical vacuum pump. The rate at which ethanol was pumped into the funnel by the syringe micropump (Cole−Parmer, 74900-20) was adjusted until the height of the liquid−vapor interface did not change by more than ±10 μm. The micropump provided a flow rate with an accuracy of 0.5% of the set rate. The system was deemed to be operating in steady state when the interface height remained steady for at least 1 h. Under steady-state conditions, the ethanol evaporation rate was equal to the flow rate provided by the micropump.

C. Measurements Made during Steady-State Evaporation. As the ethanol flowed through the funnel throat, its temperature was controlled by a heat exchanger (Haake, F2+R) and monitored by the throat thermocouple, T_{th}, that had a sheath diameter of 813 μm and was located 3.40 mm below the funnel mouth. The ethanol in the funnel throat was kept about 1 K colder than the interfacial liquid temperature. We assume that buoyancy-driven convection can be neglected in the liquid phase. In the vapor phase, buoyancy-driven convection was eliminated since the coldest place in the vapor was nearest to the liquid−vapor interface.

Once steady state was reached, the measurement procedure could be initiated. The temperatures in the liquid and vapor phases were measured with a microthermocouple attached to a positioning micrometer (Vacuum Generators, HPT040). The microthermocouple had been formed into a U-shape and had a wire diameter of 25 μm and a bead diameter of 45 μm. The micrometer had a positioning accuracy of ±10 μm in the *X*, *Y*, and *Z* directions. Temperature measurements as a function of height were made along the centerline of the funnel in the vapor

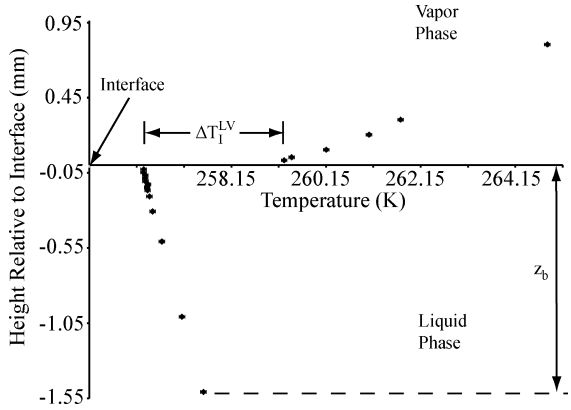

Figure 7. A typical centerline temperature profile of ethanol during steady-state evaporation. This profile was measured in experiment EthSSEV1.

and liquid phases. The interfacial vapor temperature measurements were made by placing the center of the microthermocouple bead 30 μm above the liquid−vapor interface. The interfacial liquid temperature measurements were made by first submerging the microthermocouple about 600 μm into the liquid phase to break the surface tension and then raising the microthermocouple until the center of its bead was 30 μm below the interface. All temperature measurements were recorded with a data acquisition system (Agilent, 34970A) at 3 samples per second for 1 min. All thermocouples were type K (Omega) and were calibrated from 245 to 303 K against a high-precision platinum resistance thermometer meeting NIST standards (Isotech, ASL-F100) to an accuracy of ±0.03 K. The accuracy of the throat thermocouple was ±0.04 K. The zero point of the thermocouples was maintained with calibrated ice point cells (Omega, TRCIII).

Throughout the course of an experiment, vapor-phase pressure measurements were made with two capacitance diaphragm pressure transducers (Inficon, CDG045). The transducers were also connected to the data acquisition system. One pressure transducer had a full scale of 1333 Pa and was located 200 mm above the funnel mouth. The second pressure transducer had a full scale of 13 332 Pa and was located 250 mm above the funnel mouth. The reading errors of the first and second transducers were 0.17 and 0.3%, respectively, in the pressure range between 133 and 1333 Pa. Prior to running an experiment, the zero point of the pressure transducers was calibrated down to a pressure of $\sim 10^{-5}$ Pa after the chamber was evacuated with a turbomolecular pump.

The vapor phase after each experiment was again monitored with the gas analyzer and compared to the readings made before any ethanol was introduced into the chamber. Air was the only impurity identified. The partial pressure of N_2 was $\sim 7.5 \times 10^{-5}$ Pa, and the partial pressure of ethanol was at least 2 orders of magnitude larger. At the end of an experiment, the surface tension of a sample of ethanol was measured and found to be within 2% percent of the documented value.

III. Experimental Results

A typical temperature profile on the centerline of the evaporating ethanol is shown in Figure 7. The temperature of the liquid phase is coldest at the interface and increases linearly with depth. Due to the shape of the thermocouple and the stainless-steel funnel, the temperature of the liquid phase could not be measured at depths greater than 1.8 mm. In the vapor phase, the temperature was lowest at the interface and increased with height. A temperature discontinuity ($\Delta T_I^{LV} \equiv T_I^V - T_I^L$) was observed at the liquid−vapor interface in which the interfacial vapor temperature was greater than that of the liquid. Similar temperature discontinuities have been observed in kinetic studies involving other fluids.[1,2,10,13,28]

Table 1 lists the experimental conditions measured on the funnel centerline during the steady-state evaporation of ethanol. The error in the temperature measurement at a point was taken to be the standard deviation of 150 measurements made at each position. The error in the position measurement was ±10 μm. Note that according to Table 1, the interfacial vapor temperature measurements were made within 2 to 7 mean-free paths (MFP) of the interface. We will assume that these are the interfacial vapor temperatures.

TABLE 1: Experimental Conditions in the Liquid and Vapor Phases on the Funnel Centerline that were Measured during the Steady-State Evaporation of Ethanol

experiment	$P_I^V \pm$ SD[a] (Pa)	$T_I^L \pm$ SD (K)	$T_I^V \pm$ SD (K)	$T_{th} \pm$ SD (K)	j_{ev}^0 (mg/m^{2}s)	z_m (mm)	MPF (μm)	$P_s(T)$[b] (Pa)	ΔT_I^{LV}[c] (K)
EthSSEV1	399.00 ± 0.67	256.30 ± 0.04	259.82 ± 0.05	256.21 ± 0.01	264.785	0.98	9.01	399.34	3.52 ± 0.08
EthSSEV2	497.00 ± 0.61	258.88 ± 0.04	261.65 ± 0.05	258.10 ± 0.01	104.271	0.98	7.31	497.23	2.77 ± 0.08
EthSSEV3	866.20 ± 2.63	266.02 ± 0.05	268.39 ± 0.05	265.29 ± 0.03	140.944	1.06	4.35	866.49	2.37 ± 0.08
EthSSEV4	778.00 ± 1.34	264.56 ± 0.05	266.99 ± 0.04	263.42 ± 0.03	115.209	1.06	4.81	778.27	2.43 ± 0.08
EthSSEV5	637.00 ± 1.51	262.13 ± 0.05	264.88 ± 0.03	260.86 ± 0.04	123.366	1.06	5.80	637.29	2.75 ± 0.07
EthSSEV6	231.68 ± 2.32	249.06 ± 0.04	253.37 ± 0.05	249.44 ± 0.18	224.346	1.05	14.94	231.98	4.31 ± 0.08
EthSSEV7	242.88 ± 2.87	250.03 ± 0.04	253.92 ± 0.05	248.84 ± 0.14	24.359	1.65	14.30	243.09	3.89 ± 0.08
EthSSEV8	256.36 ± 3.60	250.60 ± 0.05	254.64 ± 0.06	248.95 ± 0.16	102.461	1.94	13.61	256.62	4.04 ± 0.09
EthSSEV9	253.90 ± 3.05	250.61 ± 0.04	254.59 ± 0.05	248.88 ± 0.12	157.475	1.94	13.73	254.16	3.98 ± 0.08
EthSSEV10	374.34 ± 1.25	255.60 ± 0.04	258.82 ± 0.05	254.26 ± 0.04	191.121	0.96	9.54	374.60	3.21 ± 0.08
EthSSEV11	432.44 ± 0.90	257.38 ± 0.05	260.58 ± 0.05	256.01 ± 0.04	141.335	2.99	8.35	432.71	3.20 ± 0.08
EthSSEV12	502.35 ± 2.58	258.87 ± 0.04	261.62 ± 0.04	257.46 ± 0.06	79.983	0.97	7.23	502.57	2.75 ± 0.07
EthSSEV13	669.74 ± 1.46	262.29 ± 0.04	264.71 ± 0.16	261.22 ± 0.08	96.155	0.66	5.51	669.97	2.42 ± 0.17
EthSSEV14	621.38 ± 0.97	261.62 ± 0.04	263.82 ± 0.08	260.41 ± 0.02	114.794	0.74	5.91	621.56	2.20 ± 0.10
EthSSEV15	577.62 ± 1.62	260.81 ± 0.05	263.21 ± 0.05	259.53 ± 0.04	110.835	0.74	6.34	577.82	2.40 ± 0.08
EthSSEV16	537.15 ± 2.14	258.87 ± 0.05	261.62 ± 0.06	258.56 ± 0.04	79.983	0.97	7.23	537.35	2.47 ± 0.09
EthSSEV17	282.18 ± 1.09	252.03 ± 0.05	256.08 ± 0.06	251.38 ± 0.05	172.975	1.81	12.46	282.48	4.05 ± 0.09
EthSSEV18	289.61 ± 1.87	252.36 ± 0.05	256.37 ± 0.05	251.95 ± 0.10	172.365	2.28	12.16	289.91	4.01 ± 0.08
EthSSEV19	294.57 ± 1.15	252.62 ± 0.04	256.52 ± 0.05	252.81 ± 0.01	171.671	1.30	11.97	294.86	3.90 ± 0.08
EthSSEV20	289.42 ± 0.53	252.53 ± 0.04	256.65 ± 0.05	253.94 ± 0.03	234.597	1.85	12.19	289.75	4.12 ± 0.08
EthSSEV21	385.51 ± 0.32	256.37 ± 0.04	259.78 ± 0.05	255.93 ± 0.01	166.083	1.81	9.32	385.79	3.41 ± 0.08
EthSSEV22	396.58 ± 0.67	256.88 ± 0.04	260.33 ± 0.06	256.74 ± 0.01	210.547	1.60	9.09	396.64	3.45 ± 0.08

[a] SD is the standard deviation. [b] SRT-predicted value of $P_s(T)$. [c] Measured interfacial temperature discontinuity.

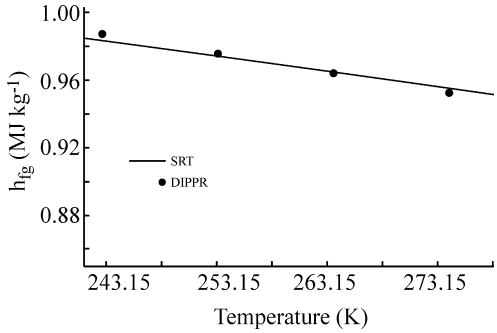

Figure 8. Comparison of the predicted values of $h_{fg}(T)$ obtained from $f_{srt}^{eth}(T)$ with the independently determined values reported by DIPPR[15,29] in the temperature range considered.

The interface size can be calculated from knowledge of the radius of the funnel mouth, x_m, and the height of the ethanol above the funnel mouth, z_m. Since the interface is approximately spherical, its curvature on the centerline, C_0, can be determined from

$$C_0 = \frac{2z_m}{z_m^2 + x_m^2} \tag{15}$$

To investigate the effect of a nonspherical interface in the application of SRT, several experiments were conducted where $z_m > 1$ mm and did not indicate any effect on the SRT results.

The difference in enthalpies in eq 3 can be computed by using the constant-pressure specific heats of the vapor and liquid phases and calculating the change from their values at the triple-point temperature, T_{tp}. If the enthalpy of vaporization at T_{tp} is $h_{fg}(T_{tp})$, then the denominator of eq 3 becomes

$$h^V(T_I^V) - h^L(T_I^L) = h_{fg}(T_{tp}) + c_p^V(T_{tp})\cdot(T_I^V - T_{tp}) - c_p^L(T_{tp})\cdot(T_I^L - T_{tp}) \tag{16}$$

Thus, by measuring the temperature gradients in the liquid and vapor phases and evaluating the fluid properties, the local centerline j_{ev}^0 can be calculated from eqs 3 and 16, and the values of j_{ev}^0 are given in Table 1. Fluid properties used in the calculations are given in the Appendix.

A. Saturation Vapor Pressure Determined from SRT. Since the measured experimental conditions (T_I^V, T_I^L, P_I^V, j_{ev}^0, C_0) and the fluid properties (ν_f, γ^{LV}, ω_l) are known for all experiments, SRT can be applied at the centerline to calculate the $P_s(T)$ value for each experiment. The results are shown as open circles in Figure 1. An analytical expression for $f_{srt}^{eth}(T)$ was formulated from the SRT-calculated $P_s(T)$ values

$$f_{srt}^{eth}(T) = \exp\left[52.165 - \frac{6445}{T} - 3.75424 \times \ln[T] - 3.0053 \times 10^{-6}(T^2 - T)\right] \tag{17}$$

where $f_{srt}^{eth}(T)$ is in Pa and T is in K. A curve calculated from $f_{srt}^{eth}(T)$ is shown in Figure 1 and is about 10% below the DIPPR, Yaws, and Dillon and Penoncello $P_s(T)$ curves.

B. Calculation of $h_{fg}(T)$ and $c_p^L(T)$ from $f_{srt}^{eth}(T)$. The evaporative latent heat predicted from SRT was calculated by inserting eq 17 into eq 12. The $h_{fg}(T)$ values predicted from $f_{srt}^{eth}(T)$ are plotted in Figure 8 where they may be compared with the available data for $h_{fg}(T)$. Note that there is no disagreement between the predicted and independently determined values[15,29] in the temperature range between 243 and 273 K.

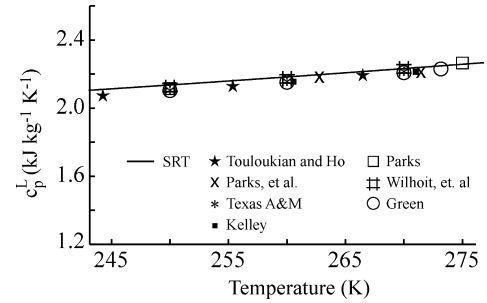

Figure 9. Comparison of the predicted values of $c_p^L(T)$ obtained from $f_{srt}^{eth}(T)$ with the independently measured values available in the literature in the temperature range considered.

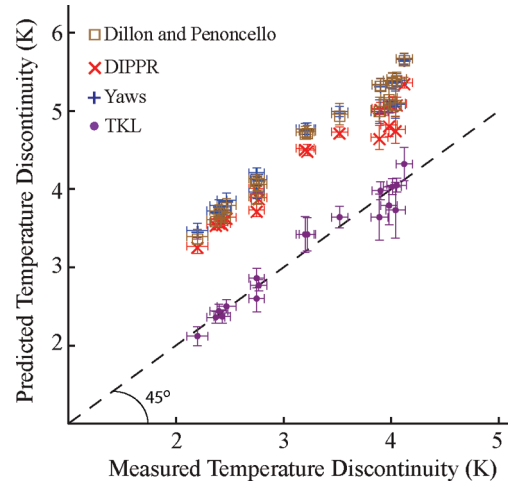

Figure 10. Predictions of the liquid−vapor interfacial temperature discontinuities.

The $c_p^L(T)$ values predicted from the $P_s(T)$ expressions of DIPPR, Yaws, and Dillon and Penoncello have already been presented in Figure 3. The SRT-predicted $c_p^L(T)$ curve is found by substituting $f_{srt}^{eth}(T)$ into eq 13 and is shown in Figure 9. The $c_p^L(T)$ values determined from $f_{srt}^{eth}(T)$ agree with the independently measured values for temperatures in the range of $243 < T < 273$ K. Only $f_{srt}^{eth}(T)$ leads to correct predictions of both $h_{fg}(T)$ and $c_p^L(T)$.

C. Prediction of the Measured Interfacial Temperature Discontinuities. The $f_{srt}^{eth}(T)$ expression was the only one to correctly predict both $h_{fg}(T)$ and $c_p^L(T)$ of ethanol at low temperatures. Another test of this expression is to use it in SRT to predict the temperature discontinuities at the liquid−vapor interface, ΔT_I^{LV}. One experiment is shown in Figure 7, and the values for the other experiments are listed in Table 1.

If the fluid properties ($P_s(T) = f_{srt}^{eth}(T)$, ν_f, γ^{LV}, ω_l) and experimental conditions (T_I^V, P_I^V, j_{ev}^0, C_0) are specified, then SRT can be solved for T_I^L, and ΔT_I^{LV} can be computed and compared to the measured experimental value. To predict ΔT_I^{LV}, an iterative procedure is followed. The procedure begins by assuming a value of T_I^L. Equation 4 is solved for the vapor-phase pressure, P_{calc}^V. This calculated value is then compared to the measured P_I^V value. If the two values are different, a new value of T_I^L is assumed, and the process is repeated. The process is continued until P_{calc}^V is equal to P_I^V. The T_I^L value that satisfies this condition is then used to calculate ΔT_I^{LV}.

TABLE 2: Values of P^{V}_{pred}, Δs_{lv}, Δs_{ct}, Δs_{ph}, $\Delta s_{\Delta T}$, and Δs_{ω_i} for the Series of Steady-State Ethanol Evaporation Experiments Listed in Table 1[a]

experiment	P^{V}_{pred} (Pa)	$(\Delta s_{lv}/k_b) \times 10^6$	$(\Delta s_{ct}/k_b) \times 10^6$	$(\Delta s_{ph}/k_b) \times 10^6$	$(\Delta s_{\Delta T}/k_b) \times 10^6$	$(\Delta s_{\omega_i}/k_b) \times 10^6$
EthSSEV1	402.975	176.978	842.248	−665.270	−373.822	−291.448
EthSSEV2	496.842	56.830	463.596	−406.766	−227.357	−179.409
EthSSEV3	865.427	44.710	332.025	−287.315	−157.808	−129.508
EthSSEV4	774.714	40.713	344.947	−304.235	−167.705	−136.530
EthSSEV5	642.290	52.337	446.660	−394.324	−218.594	−175.730
EthSSEV6	218.322	272.711	1308.550	−1035.840	−592.109	−443.733
EthSSEV7	237.641	27.264	866.969	−839.705	−479.148	−360.558
EthSSEV8	249.596	109.310	1012.120	−902.806	−514.273	−388.533
EthSSEV9	249.803	167.863	1044.050	−876.191	−499.150	−377.040
EthSSEV10	380.504	135.121	694.014	−558.893	−314.769	−244.125
EthSSEV11	440.165	86.683	633.563	−546.881	−306.619	−240.262
EthSSEV12	496.453	43.626	444.567	−400.941	−224.114	−176.827
EthSSEV13	650.406	40.300	345.501	−305.201	−169.214	−135.987
EthSSEV14	617.306	50.630	303.766	−253.136	−140.639	−112.497
EthSSEV15	579.240	52.013	354.460	−302.447	−168.325	−134.121
EthSSEV16	538.579	40.296	362.134	−321.838	−179.516	−142.321
EthSSEV17	282.082	163.744	1064.090	−900.341	−510.992	−389.350
EthSSEV18	290.107	158.760	1039.880	−881.124	−499.698	−381.426
EthSSEV19	296.583	154.756	987.132	−832.375	−471.827	−360.549
EthSSEV20	294.286	213.063	1142.260	−929.193	−526.631	−402.562
EthSSEV21	405.336	110.386	734.558	−624.172	−350.731	−273.441
EthSSEV22	422.565	134.362	771.546	−637.184	−357.553	−279.631

[a] Note that $\Delta s_{lv} = \Delta s_{ct} + \Delta s_{ph}$ and $\Delta s_{ph} = \Delta s_{\Delta T} + \Delta s_{\omega_i}$.

The results of this calculation are shown as dots in Figure 10. The maximum ΔT_I^{LV} measured was 4.31 K. The predicted values of ΔT_I^{LV} that are in perfect agreement with the measured values would lie on the 45° line. As can be seen in Figure 10, the measured ΔT_I^{LV} values and those predicted using $f^{eth}_{srt}(T)$ lie on this line within the experimental error. The horizontal error bars reflect the unsteadiness of the interface during the experiments. These are relatively small since the interface did not move by more than ±10 μm throughout the course of an experiment. The vertical error bars reflect the fluctuations in the measured vapor-phase pressure and the fitting errors introduced by formulating the expression for $f^{eth}_{srt}(T)$. The predictions of ΔT_I^{LV} made from experiment EthSSEV13 are not shown in Figure 10 since the standard deviation of the measured T_I^{V} was 0.16 K and was about three times greater than the standard deviation of the other experiments.

These calculations have been repeated using the $P_s(T)$ expressions from DIPPR, Yaws, and Dillon and Penoncello. The results are also shown in Figure 10. It is apparent that only $f^{eth}_{srt}(T)$ leads to correct predictions of the measured ΔT_I^{LV} values for all experiments.

IV. Discussion

A series of 22 steady-state evaporation studies of ethanol have been performed. An expression for the saturation vapor pressure of ethanol, $f^{eth}_{srt}(T)$, was formulated from SRT. The average of the sum of the errors between $f^{eth}_{srt}(T)$ and the 22 calculated $P_s(T)$ values was 1.7%. A large part of this error came from three experiments (EthSSEV6, EthSSEV21, and EhSSEV22). These data points were scattered about $f^{eth}_{srt}(T)$ and accounted for 41% of the overall error. For this reason, we omit experiments EthSSEV6, EthSSEV21, and EhSSEV22 from the discussion that follows and note that the average of the sum of the errors between $f^{eth}_{srt}(T)$ and the 19 calculated $P_s(T)$ values is 1.0%.

The $f^{eth}_{srt}(T)$ expression correctly predicted the $h_{fg}(T)$ values determined independently, as indicated in Figure 8. Accurate, low-temperature data were not available in the literature. Instead, the independent data used in Figure 8 were calculated from the Clapeyron equation.[15,29] The average error between the $h_{fg}(T)$ values predicted from SRT and those independently calculated was 0.3%.

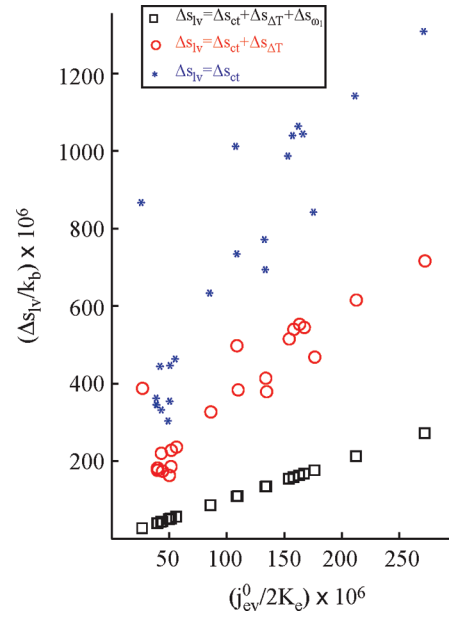

Figure 11. Nondimensional plot of predicted Δs_{lv} values for measured values of j^0_{ev}. Three cases are considered, when Δs_{lv} was calculated with all terms (squares), without the phonon terms (circles), and without the temperature discontinuity and phonon terms (stars).

The SRT prediction of $c^L_p(T)$ also agreed with the independent experimental data to 0.7% over the temperature range from 243 to 273 K, as shown in Figure 9. Independent measurements of $c^L_p(T)$ values were accurately obtained by others. The measurement error of the independent $c^L_p(T)$ values was between 0.5 and 3%.[15,21,30−34] Thus, the independent $c^L_p(T)$ values provided a stringent test of the expression for $f^{eth}_{srt}(T)$.

The $f^{eth}_{srt}(T)$ expression was the only one to correctly predict both the $h_{fg}(T)$ and $c^L_p(T)$ values of ethanol. These results indicate

TABLE 3: Three $P_s(T)$ Expressions for Ethanol, where T is in K and P_s is in Pa

source	saturation vapor pressure
DIPPR[15]	$P_s(T) = \exp\left[73.304 - \frac{7122.3}{T} - 7.1424 \times \ln[T] + 2.8853 \times 10^{-6} T^2\right]$
Yaws[16]	$P_s(T) = 133.3224 \times 10^{(23.844 - 2864.2/T - 5.0474 \times \log_{10}[T] + 3.7448 \times 10^{-11} T + 2.7361 \times 10^{-7} T^2)}$
Dillon and Penoncello[17]	$P_s(T) = 6.137 \times 10^6 \times \exp\left[\frac{514}{T}\left(-0.0514771\left(1 - \frac{T}{514}\right)^{1/2} - 8.27075\left(1 - \frac{T}{514}\right) - 5.49245\left(1 - \frac{T}{514}\right)^3 + 5.64829\left(1 - \frac{T}{514}\right)^{11/2}\right)\right]$

TABLE 4: Fluid Properties of Ethanol given by DIPPR[15a]

property	expression or value	unit
triple point temperature	$T_{tp} = 159.05$	(K)
dynamic viscosity of vapor	$\nu^V(T) = \frac{1.0613 \times 10^{-7} T^{0.8066}}{1 + \frac{52.7}{T}}$	(Pa·s)
latent heat at triple point	$h_{fg}(T_{tp}) = 1.07871 \times 10^6$	(J/kg)
specific heat liquid	$c_p^L(T) = \frac{102640 - 139.63T - 0.030341T^2 + 0.0020386T^3}{46.06844}$	(J/kg·K)
specific heat of vapor	$c_p^V(T) = \frac{49200}{46.06844} + \frac{145770}{46.06844}\left(\frac{\frac{1662.8}{T}}{\sinh\left[\frac{1662.8}{T}\right]}\right)^2 + \frac{93900}{46.06844}\left(\frac{\frac{744.7}{T}}{\cosh\left[\frac{744.7}{T}\right]}\right)^2$	(J/kg·K)
specific volume of fluid	$v_f(T) = \left(\frac{46.06844 \times 1.6288}{0.27469^{(1+(1 - T/514)^{0.23178})}}\right)^{-1}$	(m^3/kg)
surface tension	$\gamma^{LV}(T) = 0.03764 - 0.00002157T - 1.025 \times 10^{-7} T^2$	(N/m)
thermal conductivity of liquid	$\kappa^L(T) = 0.2468 - 0.0002640T$	(W/m·K)
thermal conductivity of vapor	$\kappa^V(T) = \frac{-0.010109T^{0.6475}}{1 - \frac{7332}{T} - \frac{268000}{T^2}}$	(W/m·K)

[a] T is in K.

that $f_{srt}^{eth}(T)$ has an accurate shape (slope and concavity) in the temperature range of $246 < T_I^L < 267$ K. It was also the only one to lead to correct predictions of the interfacial temperature discontinuity during ethanol evaporation. The agreement between the predicted and measured ΔT_I^{LV} shows that $f_{srt}^{eth}(T)$ is consistent with the experiments. However, a stricter test of the accuracy of $f_{srt}^{eth}(T)$ would be to predict the ΔT_I^{LV} for an independent set of steady-state ethanol evaporation studies (i.e., experiments that were not used to formulate $f_{srt}^{eth}(T)$).

A. Inconsistencies in the Saturation Vapor Pressure Expression for Ethanol Found in the Literature. Other $P_s(T)$ expressions have been analyzed in this study, but the $P_s(T)$ data available in the literature were found to be thermodynamically inconsistent. None of the other $P_s(T)$ expressions investigated correctly predicted both the $h_{fg}(T)$ and $c_p^L(T)$ of ethanol. Moreover, the predicted fluid properties made from these $P_s(T)$ expressions did not agree with each other. In addition, the $P_s(T)$ data available in the literature is open to question. For example, DIPPR presents an expression for the $P_s(T)$ of ethanol that was formulated from a selection of over 100 data sets from more than 35 investigations spanning almost 120 years.[15,35] The purity of some of these samples is open to question.

Our control of ethanol purity was through the measured surface tension of the degassed ethanol. The error was less than 2% of the documented value. Also, the composition of the vapor phase determined from a quadrupole residual gas analyzer indicated that air was the only measurable impurity, and its partial pressure was 2 orders of magnitude less than that of ethanol.

Others such as Dillon and Penoncello and Lange have presented $P_s(T)$ expressions for ethanol, but the lack of low-temperature data has limited the validity of their expressions to temperatures typically above 273 K.[17,36]

B. Role of Molecular Phonons During the Evaporation of Ethanol. The change in entropy of a molecule as it leaves the liquid phase and enters the vapor phase is Δs_{lv} and was defined earlier by eq 7. This term can be written as a sum of two other terms, the change in entropy due to continuum effects, Δs_{ct}, and the change in entropy due to the interfacial temperature discontinuities and the molecular phonons, Δs_{ph}. The first term is given in eq 18. The second term is divided further into eq 19, which does not contain any phonon terms, and eq 20, where q_{vib} and θ_l are defined by eqs 8 and 9, respectively. The role of

the molecular phonons during the evaporation of ethanol may be examined by writing Δs_{ph} as the sum of $\Delta s_{\Delta T}$ and Δs_{ω_l}.

$$\frac{\Delta s_{ct}}{k_b} = \frac{v_f(T_I^L)}{k_b T_I^L}[P_I^V + \gamma^{LV}(T)\cdot 2C_0 - P_s(T_I^L)] + \ln\left[\frac{P_s(T_I^L)}{P_I^V}\right] \quad (18)$$

$$\frac{\Delta s_{\Delta T}}{k_b} = 4\left(1 - \frac{T_I^V}{T_I^L}\right) + \ln\left[\left(\frac{T_I^V}{T_I^L}\right)^4\right] \quad (19)$$

$$\frac{\Delta s_{\omega_l}}{k_b} = \left(\frac{1}{T_I^V} - \frac{1}{T_I^L}\right) \times \sum_{l=1}^{3n-6}\left[\frac{\theta_l}{2} + \frac{\theta_l}{e^{\theta_l/T_I^V} - 1}\right] + \ln\left[\frac{q_{vib}(T_I^V)}{q_{vib}(T_I^L)}\right] \quad (20)$$

In the calculation of Δs_{ct}, the $\ln[P_I^V/P_s(T)]$ term dominates. It is important to correctly determine this ratio. To eliminate any errors introduced by fitting $f_{srt}^{eth}(T)$ or measurement errors of P_I^V, the vapor-phase pressure of each experiment is predicted, P_{pred}^V, by applying SRT to the experimental conditions. Then, P_{pred}^V is used instead of P_I^V in the Δs_{ct} calculations. The values of P_{pred}^V, Δs_{lv}, Δs_{ct}, Δs_{ph}, $\Delta s_{\Delta T}$, and Δs_{ω_l} are given in Table 2.

The values in Table 2 provide insight into the role that molecular phonons play in the evaporation process. First, note that all of the Δs_{lv} values are positive. This term is the change in entropy as a result of a molecule spontaneously transferring from the liquid to the vapor. Positive values of Δs_{lv} are expected since the ethanol in all experiments was evaporating. Next, all of the Δs_{ph} terms are negative, indicating that the molecular phonons act to hinder the evaporation process. Furthermore, the magnitude of Δs_{ph} compared to that of Δs_{ct} reveals that the role of the molecular phonons in evaporation is not negligible compared to the continuum effects. These observations are consistent with those made for water.[9]

Three approximations of Δs_{lv} are illustrated in Figure 11 for different measured values of $j_{ev}^0/2K_e$. We can see that omitting the phonon terms has the effect of increasing the value of Δs_{lv} for all of the experimental conditions considered. If the Δs_{ph} term is completely neglected, the increase in Δs_{lv} is even more pronounced. Therefore, the interfacial temperature discontinuity and phonon contributions to the entropy change, Δs_{ph}, are significant and have a strong effect on the predicted evaporation rate.

V. Conclusion

A series of low-temperature ($246 < T_I^L < 267$ K) steady-state ethanol evaporation studies has been conducted. The measured interfacial conditions have been used in SRT to predict an expression for the saturation vapor pressure, $f_{srt}^{eth}(T)$. This expression has led to predictions of the latent heat, $h_{fg}(T)$, and the liquid-phase constant-pressure specific heat, $c_p^L(T)$, that are consistent with independently determined values of these properties.

A positive interfacial temperature discontinuity ($\Delta T_I^{LV} \equiv T_I^V - T_I^L$) was measured across the liquid−vapor interface in all experiments, and SRT was successfully applied to predict ΔT_I^{LV}. The calculation requires an accurate $P_s(T)$ expression for ethanol. Other $P_s(T)$ expressions from the literature were investigated, but $f_{srt}^{eth}(T)$ was the only one found to be thermodynamically consistent and the only one to lead to correct predictions of ΔT_I^{LV}. The agreement between the predicted fluid properties, $h_{fg}(T)$ and $c_p^L(T)$, and their independent measurements and between the predicted and measured ΔT_I^{LV} suggest that the measured interfacial temperatures made with the microthermocouple are sufficiently accurate to use in SRT.

Acknowledgment. We gratefully acknowledge the support of the Canadian Space Agency, the Natural Sciences and Engineering Research Council of Canada, and the European Space Agency.

Appendix

The three $P_s(T)$ expressions of ethanol found in the literature and investigated in this study are given in Table 3.

The mean-free path can be approximated from

$$\mathrm{MFP} = \frac{10^6 k_b T_I^V}{\sqrt{2}\pi P_I^V (d(T_I^V))^2} \quad (21)$$

where MFP is in μm, N_A is Avogadro's number, and $d(T_I^V)$ is the theoretical diameter of a molecule in the hard-sphere approximation. The diameter of an ethanol molecule can be determined from[37]

$$d(T_I^V) = \left(\frac{46.06844 k_b T_I^V}{6(\pi \nu^V(T_I^V))^2 N_A \times 10^3}\right)^{1/4} \quad (22)$$

where $d(T_I^V)$ is in m and $\nu^V(T_I^V)$ is the dynamic viscosity of the vapor.

The fluid properties of ethanol used in this study are listed in Table 4. The properties are taken from DIPPR.[15]

References and Notes

(1) Fang, G.; Ward, C. A. *Phys. Rev. E* **1999**, *59*, 417.
(2) Ward, C. A.; Stanga, D. *Phys. Rev. E* **2001**, *64*, 051509.
(3) Ward, C. A.; Duan, F. *Phys. Rev. E* **2004**, *69*, 056308.
(4) Duan, F.; Thompson, I.; Ward, C. A. *J. Phys. Chem. B* **2008**, *112*, 8605.
(5) Thompson, I.; Duan, F.; Ward, C. A. *Phys. Rev. E* **2009**, *80*, 056308.
(6) Ward, C. A. *J. Chem. Phys.* **1983**, *79*, 5605.
(7) Ward, C. A.; Findlay, R. D.; Rizk, M. *J. Chem. Phys.* **1982**, *76*, 5599.
(8) Ward, C. A.; Fang, G. *Phys. Rev. E* **1999**, *59*, 429.
(9) Duan, F.; Ward, C. A.; Badam, V. K.; Durst, F. *Phys. Rev. E* **2008**, *78*, 041130.
(10) Fang, G.; Ward, C. A. *Phys. Rev. E* **1999**, *59*, 441.
(11) Kapoor, A.; Elliott, J. A. W. *J. Phys. Chem. B* **2008**, *112*, 15005.
(12) Peng, D.-Y.; Robinson, D. B. *Ind. Eng. Chem. Fundam.* **1976**, *15*, 59.
(13) Badam, V. K.; Kumar, V.; Durst, F.; Danov, K. *Exp. Therm. Fluid Sci.* **2007**, *32*, 276.
(14) Badam, V. K. Ph.D. Thesis, University of Erlangen, Nuremberg, Germany, 2007.
(15) *DIPPR Project 801, Full version (electronic resource): Evaluated Standard Thermophysical Property Values*; Design Institute for Physical Property Data/AIChE: Provo, UT, 2009.
(16) Yaws, C. L. *Yaws' Handbook of Thermodynamic and Physical Properties of Chemical Compounds*, electronic resource; Knovel: New York, 2004.
(17) Dillon, H. E.; Penoncello, S. G. *Int. J. Thermophys.* **2004**, *25*, 321.
(18) Duan, F.; Ward, C. A. *Phys. Rev. E* **2005**, *72*, 056302.
(19) Schmeling, T.; Strey, R. *Ber. Bunsen-Ges. Phys. Chem.* **1983**, *87*, 871.
(20) Barrow, G. M. *J. Chem. Phys.* **1952**, *20* (11), 1739.

(21) Green, J. H. S. *Trans. Faraday Soc.* **1961**, *57*, 2132.
(22) Herzberg, G. *Molecular Spectra and Molecular Structure*; Van Nostrand: Princeton, NJ, 1964; Vol. 2, p 281.
(23) Laenen, R.; Rauscher, C. *J. Mol. Struct.* **1998**, *448*, 115.
(24) Ehbrecht, M.; Huisken, F. *J. Phys. Chem. A* **1997**, *101*, 7768.
(25) Hill, T. L., *An Introduction to Statistical Thermodynamics*; Dover: Mineola, NY, 1986.
(26) Durig, J. R.; Larsen, R. A. *J. Mol. Struct.* **1989**, *238*, 195.
(27) Sasges, M. R.; Ward, C. A.; Azuma, H.; Yoshihara, S. *J. Appl. Phys.* **1996**, *79*, 8770.
(28) Duan, F.; Ward, C. A. *Phys. Rev. E* **2005**, *72*, 056304.
(29) Potter, J. H. *J. Franklin Inst.* **1966**, *281*, 423.
(30) Kelley, K. K. *J. Am. Chem. Soc.* **1929**, *51* (3), .
(31) Parks, G. S. *J. Am. Chem. Soc.* **1925**, *47*, 338.
(32) Gibson, G. E.; Parks, G. S.; Latimer, W. M. *J. Am. Chem. Soc.* **1920**, *42*, 1542.
(33) Wilhoit, R. C.; Hall, K. R.; Chao, J. *J. Phys. Chem. Ref. Data* **1985**, *14*, 1.
(34) Touloukian, Y. S., Ho, C. Y., Eds. *Thermophysical Properties of Matter*; IFI/Plenum: New York, 1970−1979.
(35) *TRC Thermodynamic Tables Hydrocarbons*; Thermodynamics Research Center, Texas A&M University: College Station, TX, 2008.
(36) Speight, J. G., Ed. *Lange's Handbook of Chemistry*, 16th ed.; McGraw-Hill: New York, 2005.
(37) Present, R. D. *Kinetic Theory of Gases*; McGraw-Hill: New York, 1958.

JP100441M